Multilayered Solid Polymer Electrolytes with Sacrificial Coating for Suppressing Lithium Dendrite Growth

Xiaowei Li,[†,‡] Yongwei Zheng,[‡] William R. Fullerton,[‡] and Christopher Y. Li[‡]*

[†] School of Materials Science and Engineering, Jiangsu University, Zhenjiang, Jiangsu 212013, China

[‡] Department of Materials Science and Engineering, Drexel University, Philadelphia, PA 19104, USA

KEYWORDS: solid polymer electrolytes, network solid polymer electrolytes, multilayered films, lithium metal batteries, lithium dendrites

ABSTRACT: The practical application of lithium metal batteries (LMBs) is hindered by the lithium dendrite formation during cycling. In this work, we report a multilayered solid polymer electrolyte (SPE) formed by sandwiching a comb-chain crosslinker-based network SPE (ConSPE) film with linear PEO SPE coating. Benefiting from the drastically different lithium dendrite resisting properties of the ConSPE and linear PEO SPE, the lithium dendrite growth in the multilayered SPEs could be tuned, with the linear PEO SPE effectively serving as a sacrificial

layer to accommodate the lithium dendrite growth. Symmetrical lithium cells with the multilayered SPE exhibited an extended short-circuit time ~ 4.1 times that for the single-layer ConSPE at a high current density of 1.5 mA cm^{-2}. Li/$LiFePO_4$ batteries with the multilayered SPEs delivered superior cycling performance at extremely high C-rates of 2 C and 10 C. Our multilayered SPE architecture, therefore, opens up a new gateway for advancing SPE design for future LMBs.

1. Introduction

Lithium metal is regarded as one of the most promising anode materials for the next-generation high-energy-density energy storage systems due to its extremely high capacity (3860 mAh g^{-1}) and lowest anode potential (-3.04 V vs. standard hydrogen electrode). The major roadblocks to the practical application of lithium metal batteries (LMBs) are the high reactivity of lithium and uncontrollable dendritic formation during battery cycling.[1, 2] To suppress lithium dendrite growth during LMB operation, a variety of strategies have been reported, such as tuning the composition of the electrolytes with tailor-designed solvents, salts, and additives,[3-5] pre-treating lithium surface,[6, 7] surface coating,[8-10] employing solid electrolytes,[11-18] and constructing three-dimensional (3D) anodes with lithium-plated matrices.[19-21] In general, these strategies are designed to homogenize current distribution, facilitate the formation of stable solid electrolyte interfaces (SEIs), or mechanically block the lithium dendrite growth.

Replacing liquid electrolytes with solid polymer electrolytes (SPEs) is a promising way to smooth lithium electrodeposition and resist lithium dendrite growth.[22-24] Compared with their ceramic counterparts, SPEs have demonstrated attractive propensities of low flammability, leak-free, high thermal stability, and enhanced energy density, as well as good flexibility and

processability.[11, 13, 25] Polymers can also be used as a coating layer to improve LMB performance. To this end, polymers such as poly(vinylidene fluoride-co-hexafluoropropylene),[26] poly(dimethylsiloxane),[27] viscoelastic self-healing polymer,[28] Nafion/polyvinylidene difluoride polymer blend,[8] and cross-linked polymer[29] have been used to stabilize the lithium/electrolyte interface. Compared with inorganic surface coating, the polymer coating is more compatible with the significant volumetric change of the electrode during cycling and more straightforward to synthesize and process.[30] Studies show that the chemistry of the polymer coating with higher dielectric constant and lower surface energy would promote larger lithium deposits due to increased lithium/coating interfacial energy and exchange current.[24] In addition, electrospun polyimide mats were also employed as a matrix in the 3D anode for accommodating lithium plating, with which uniform lithium stripping/plating was enabled.[19] Despite these extensive efforts, lithium dendrite resistance of SPEs at high current densities remains a major obstacle to achieving practical dendrite-free LMBs.

To further improve the lithium dendrite resistance and extend the cycling lifetime for SPEs, in this work, inspired by the 3D anodes that can accommodate lithium deposition, we propose a new concept of multilayered SPEs with sacrificial coating on preformed homogenous SPEs. The multilayered SPEs in this design are composed of a robust central SPE membrane that can effectively hinder lithium dendrite growth and two surface sacrificial layers that are prone to lithium dendrite formation. The sacrificial layers, therefore, provide a finite space to accommodate lithium deposition and direct dendrite growth away from the SEI normal direction so that cell short-circuit can be avoided/delayed. In this study, the ***co***mb-chain crosslinker-based ***n***etwork SPE (ConSPE) developed in our previous work was employed as the standard SPE system due to its outstanding lithium dendrite resistance compared with other SPEs.[31] A SPE membrane composed

of linear polyethylene oxide (PEO) and lithium salt was employed as the sacrificial layer due to its propensity of lithium dendrite growth compared with the ConSPE. Symmetrical lithium cells with the multilayered SPE showed prolonged lifetimes compared with the single-layer ConSPE at high current densities of 1.0 and 1.5 mA cm^{-2}, as well as excellent cycling performance and improved capacity retention for full LMBs. In addition, this concept was demonstrated using two different lithium salts, namely lithium bis(trifluoromethanesulfonyl)imide (LiTFSI) and lithium bis(fluorosulfonyl)imide (LiFSI).

2. Experimental Section

2.1. Materials

Poly(glycidyl methacrylate) (PGMA, M_n 10-20 kDa, poly(ethylene glycol) diamine (PEG, M_n 2 kDa), poly(ethylene oxide) (PEO, average M_v 300 kDa), lithium bis(trifluoromethane)sulfonimide (LiTFSI) and tetrahydrofuran (THF) were purchased from Sigma-Aldrich. Lithium bis(fluorosulfonyl)imide (LiFSI) was purchased from TCI. Lithium foil was obtained from Alfa Aesar. $LiFePO_4$ and super P were purchased from MTI.

2.2. Preparation of multilayered SPEs

The comb-chain crosslinker PGMA-based network SPEs (ConSPEs) were prepared according to the previous report.[31] The molar ratio of PGMA monomer/PEG is 2, and molar ratio of EO/Li^+ is 16 for ConSPEs. The thickness of the ConSPE films was controlled by changing the total mass of PGMA, PEG, and LiTFSI on the fixed-size glass slice, and two ConSPE films with a thickness of 120 and 170 μm were prepared.

PEO-LiTFSI and PEO-LiFSI SPEs were prepared by dissolving PEO and LiTFSI/LiFSI (molar ration of EO/Li = 20) in acetonitrile. The solution was cast on a PTFE slide and dried under vacuum

at 70 °C for over 48 h after evaporating most of the solvent at ambient temperature. The prepared membranes were stored in a glovebox before tests.

2.3. Characterization

Differential scanning calorimetry (DSC) was conducted under N_2 atmosphere using a heating/cooling rate of 10 °C min^{-1}. X-ray photoelectron spectroscopy (XPS, Physical Electronics VersaProbe 5000) experiments were conducted to probe the Li/SPE interface. C 1s at 284.8 eV was employed to calibrate the binding energy. Ionic conductivity of the SPEs were tested using AC impedance spectroscopy with a Princeton Applied Research Parstat 2273 Potentiostat. The electrochemical stability was tested by linear sweep voltammetry (LSV) at 90 °C under a rate of 1 mV s^{-1}.

Symmetrical Li cells and Li|Cu cells were assembled in the glovebox using 2032-coin cell cases with single-layer or multilayered SPEs between two Li foils or Li/Cu foils. Celgard 2400 separators with a thickness of 25 μm and a punched hole of 5 mm in diameter were placed between electrodes as the spacer, and PEO SPEs were placed in the central hole region, as shown in **Figure S1**. The cells were annealed at 90 °C for 4 hours before the stripping-plating tests.

$LiFePO_4$ cathodes were prepared using the reported method.[31] In brief, the mixture of $LiFePO_4$, PGMA-PEG precursor, and super P with a weight ratio of 60/32/8 in THF/H_2O was cast onto a stainless steel plate and dried at 120 °C under vacuum. The active material loading is 2-2.5 mg cm^{-2}. $LiFePO_4$/Li batteries were assembled in the glovebox with 2032-coin cell cases using lithium foils with a thickness of 0.75 mm as the anode, annealed at 90 °C for 4 hours and pre-cycled for 3 cycles under 0.2 C before cycling at higher rates between 2.5 and 3.8 V. The theoretical capacity of 170 mAh g^{-1} for the $LiFePO_4$ cathode was employed to determine the C-rate.

3. Results and Discussion

The ConSPE layer was prepared by crosslinking a comb-chain crosslinker poly(glycidyl methacrylate) (PGMA) and bifunctional amine-terminated polyethylene glycol (PEG) as described in our previous report (**Figure 1a**).[31] Since linear PEO melts at the operating temperature (> 60 °C, **Figure S2**) and shows a significant difference in mechanical strength and lithium dendrite resistance compared with the ConSPE, linear PEO SPEs with LiTFSI or LiFSI as the lithium salt (denoted as PEO-LiT and PEO-LiF, respectively, **Figure 1b**) were chosen as the sacrificial layer.

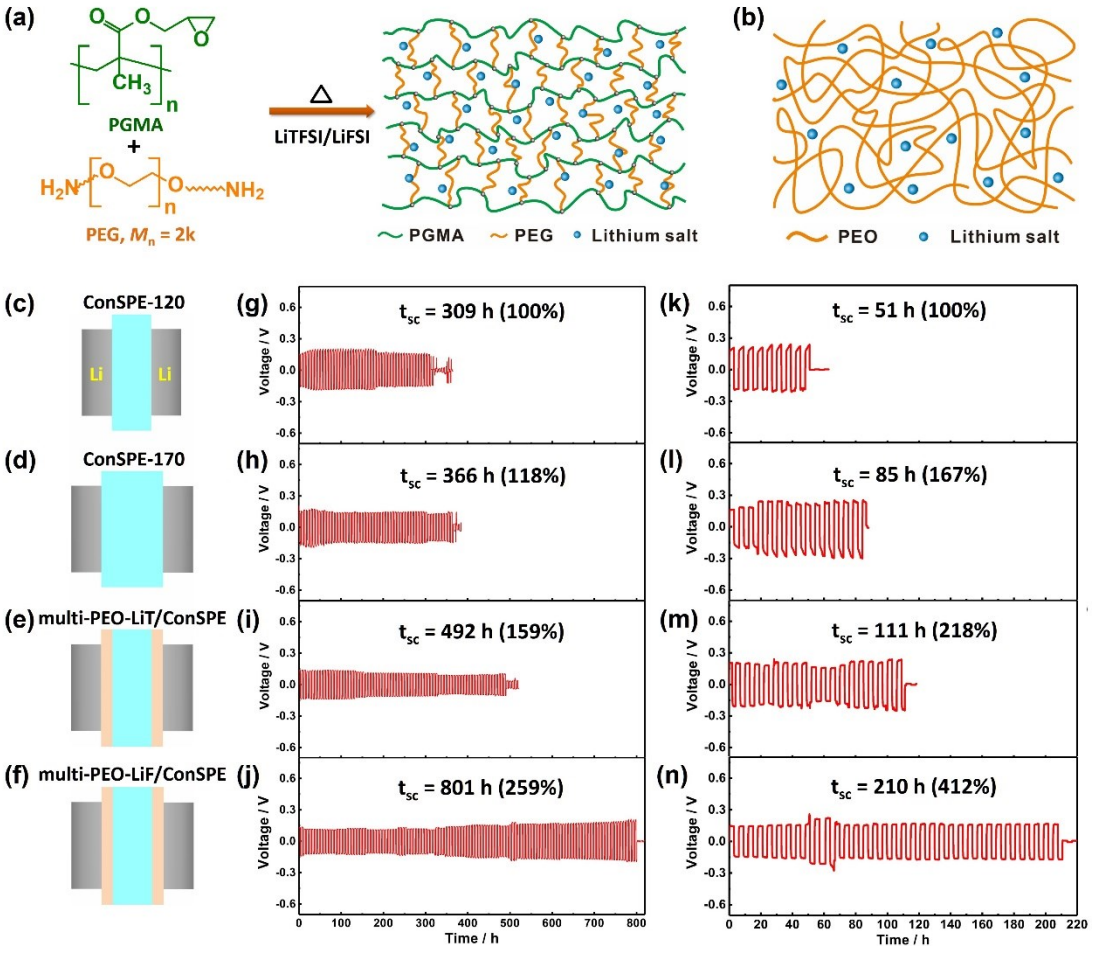

Figure 1. Schematics of (a) ConSPE and (b) PEO SPE, and symmetrical lithium cells with (c) single-layer ConSPE of 120 μm; (d) single-layer ConSPE of 170 μm; (e) multi-PEO-LiT/ConSPE; (f) multi-PEO-LiF/ConSPE, and the corresponding voltage-time profiles at 90 °C under the current density of (g-j) 1.0 mA cm^{-2} with an areal capacity of 3.0 mAh cm^{-2} and (k-n) 1.5 mA cm^{-2} with an areal capacity of 4.5 mAh cm^{-2}.

To confirm the sacrificial layer concept, three types of SPE films were prepared, as shown in **Figure 1c-e**. The first two control films are the PGMA-based ConSPEs with a thickness of 120, and 170 μm and are named ConSPE-120 and ConSPE-170, respectively. The third film is a multilayered SPE comprised of a 120 μm PGMA-based ConSPE sandwiched by two 25 μm PEO-LiT SPE, leading to a total film thickness of 170 μm. The multilayered SPE denoted as multi-PEO-LiT/ConSPE, has the same ConSPE thickness as ConSPE-120 and the same total film thickness as ConSPE-170. Symmetrical lithium cells were assembled with these SPEs sandwiched by lithium electrodes on both sides, as shown in **Figure 1** and **Figure S1**, and tested with galvanostatic charge-discharge cycling. The symmetrical lithium cells with the single-layer ConSPEs and multilayered SPE were cycled under a constant current density until the voltage suddenly dropped due to the lithium dendrite-induced short circuit. The corresponding voltage-time profiles of symmetrical lithium cells with the single-layer ConSPEs and multilayered SPE under 1.0 mA cm^{-2} with an areal capacity of 3.0 mAh cm^{-2} and under 1.5 mA cm^{-2} with an areal capacity of 4.5 mAh cm^{-2} are shown in **Figure 1g-i** and **Figure 1k-m**, respectively. Short circuit time t_{sc} is defined as the cycling time when a sudden voltage drop (> 50%) occurs. The cells exhibited a t_{sc} of 309 h under 1.0 mA cm^{-2} and 51 h under 1.5 mA cm^{-2} when a ConSPE-120 was used as the electrolyte (**Figure 1g,k**). When a thicker ConSPE-170 was used, t_{sc} increased to 366 and 85 h, respectively

(**Figure 1h,l)**, 18% and 67% higher than those for the ConSPE-120. The increase of t_{sc} with the SPE thickness is consistent with the lithium dendrite growth model by Monroe and Newman.[32, 33] When introducing 25 μm PEO-LiT SPEs between the lithium electrodes and the ConSPE-120, *i.e.* forming the multi-PEO-LiT/ConSPE, t_{sc} increased to 492 h at 1.0 mA cm^{-2}, which is 159% of the single-layer ConSPE-120. When cycled at 1.5 mA cm^{-2}, t_{sc} reached 111 h, over twice the ConSPE-120. Note that multi-PEO-LiT/ConSPE also showed significantly longer t_{sc} at both current densities compared with ConSPE-170, indicating that the increase of t_{sc} is not simply because of the increased film thickness. To delineate the effect of the sacrificial layer on the cycling lifetime, a reduced short-circuit time $t_{sc}' = t_{sc}/t_{sc0} \times 100\%$ was plotted in **Figure 2a,b**, in which t_{sc0} is the short-circuit time for the single-layer ConSPE-120. For multi-PEO-LiT/ConSPE, t_{sc}' is 159% and 218% at 1.0 and 1.5 mA cm^{-2}, respectively. Therefore, the contribution of the sacrificial layer to the improvement of lithium dendrite suppression and cycling lifetime is approximately 59% and 118% at 1.0 and 1.5 mA cm^{-2}, respectively.

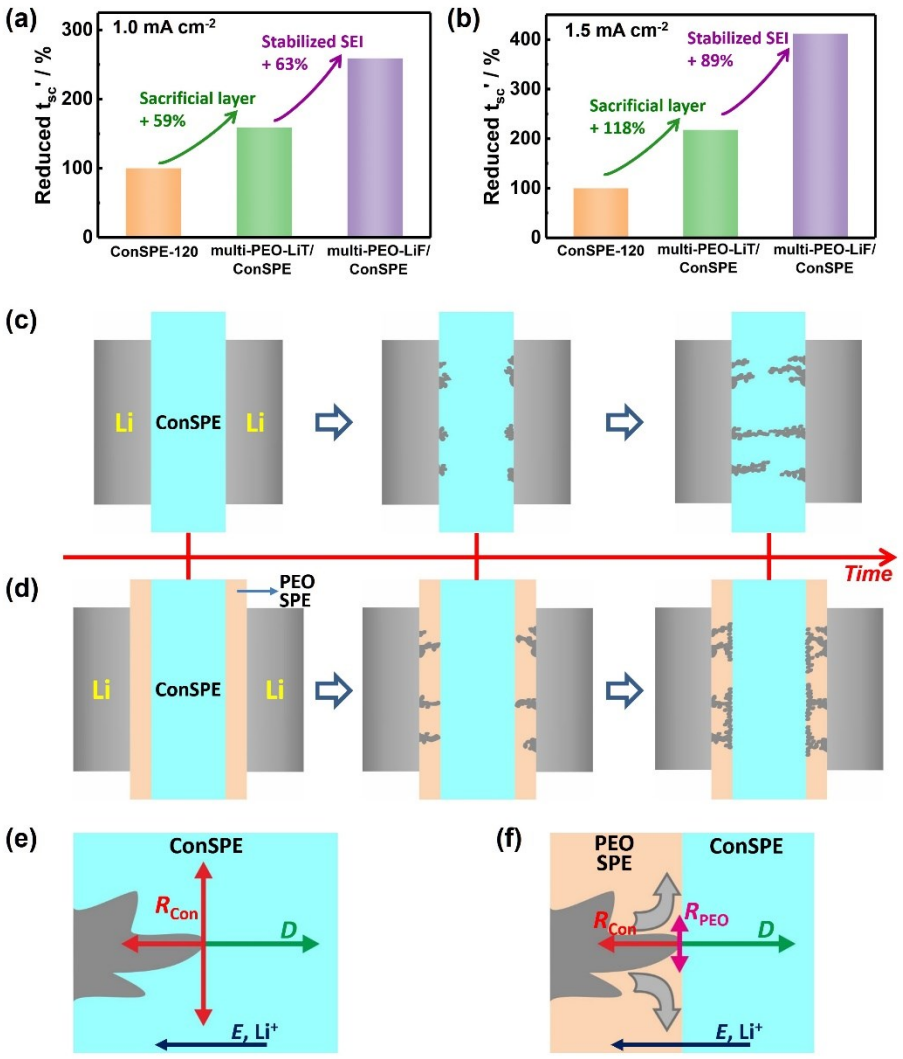

Figure 2. (a-b) Comparison of reduced short-circuit time t_{sc}' for single-layer ConSPE-120, multi-PEO-LiT/ConSPE and multi-PEO-LiF/ConSPE at the current density of (a) 1.0 mA cm^{-2} with an areal capacity of 3.0 mAh cm^{-2}, and (b) 1.5 mA cm^{-2} with an areal capacity of 4.5 mAh cm^{-2}. (c-f) show schematic of (c,d) the process and (e,f) the force analysis of the dendrite growth for (c,e) single-layer ConSPE and (d,f) multilayered SPE.

Linear PEO-based SPEs are known to have poor performance in symmetric cell tests; t_{sc} for the single-layer PEO-LiT SPE (**Figure S3**) are only 0.3 and 0.1 h at 1.0 and 1.5 mA cm^{-2}, respectively,

making little contribution to the t_{sc} for the multilayered SPE. This has been attributed to the plastic deformation of PEO melt because without crosslinking, linear PEO undergoes large deformation/flow above its melting temperature. Lithium dendrites can therefore readily pierce through the loosely entangled PEO melt and cause short-circuit, which is precisely the reason we chose PEO SPE as the sacrificial layer. The proposed mechanism for the sacrificial layer to suppress the dendrite growth and extend the cycling lifetime is displayed in **Figure 2c-f**. For the single-layer ConSPE, although its excellent lithium dendrite resistance has proven to represent the state-of-the-art,[31] the formation of uneven lithium deposition does occur. Lithium dendrite proliferation continuously takes place at the tip of the deposited lithium on account of the higher local current density.[34] The lithium deposition and dendrite growth are driven by the applied electric field (*E* in **Figure 2e,f**) and hindered by the electrically resistive SPE. In a homogeneous ConSPE, the lithium dendrite grows in the direction (shown as *D* with the green arrow in **Figure 2e,f**) with the steepest potential decay, which is generally perpendicular to the lithium electrode surface.

For the multilayered SPE, however, two interfaces were generated at the linear PEO SPE and ConSPE, where mechanical properties (at the testing temperature of 90 °C) of the SPEs significantly changed from a plastic linear PEO to an elastic ConSPE. As previously discussed, the PEO SPE can be readily penetrated by the lithium dendrite in a short time (**Figure 2d**, **Figure S3**). When the dendrite reached the interface of PEO SPE/ConSPE, the resistance to dendrite growth from PEO SPE (R_{PEO}) is weaker than that from ConSPE (R_{Con}). Therefore, the lithium dendrites are directed to grow along with the interface (**Figure 2f**). In this case, the PEO SPE acts as a sacrificial layer and provides space to accommodate the lithium dendrite growth, hence the

cycling life of the cell could be extended (**Figure 2d**). Note that this scenario closely mimics the reported 3D electrode design.[19-21]

In this study, multi-PEO-LiF/ConSPE using LiFSI instead of LiTFSI as the lithium salt in the PEO SPEs was also prepared. LiFSI has proven to be beneficial for a LiF/sulfur compounds-rich SEI formation,[35] which helps homogenize lithium electrodeposition and achieve more stable cycling.[35-38] As shown in **Figure 1j,n**, t_{sc} of multi-PEO-LiF/ConSPE increased to 801 h at 1.0 mA cm^{-2} with an areal capacity of 3.0 mAh cm^{-2}, which is a 259% increase of the single-layer ConSPE-120. When cycled at 1.5 mA cm^{-2} with an areal capacity of 4.5 mAh cm^{-2}, t_{sc} reached 210 h, over four times of the ConSPE-120. Compared with multi-PEO-LiT/ConSPE using LiTFSI as the salt, multi-PEO-LiF/ConSPE using LiFSI as the salt exhibited a much longer cycling lifetime, which is consistent with the previous reports that replacing LiTFSI in the SPEs with LiFSI could extend the cell lifetime.[35, 36] This improvement is attributed to the more stabilized LiF/sulfur compounds-rich SEI from FSI^- anions as previously reported.[35-38] Therefore, compared with the single-layer ConSPE, the superior performance of multi-PEO-LiF/ConSPE on the cycling lifetime could be attributed to the synergistic effect of the linear PEO sacrificial layer and further stabilized SEI. The reduced short-circuit time t_{sc}' plotted in **Figure 2a,b** can be used to delineate these two factors on the cycling lifetime. For multi-PEO-LiF/ConSPE, t_{sc}' is 259% and 412% at 1.0 and 1.5 mA cm^{-2}, respectively comparing with ConSPE-120. Since the contribution of the sacrificial layer to the cycling lifetime improvement obtained from t_{sc}' of multi-PEO-LiT/ConSPE is 59% and 118% at 1.0 and 1.5 mA cm^{-2}, the contribution of stabilized SEI could be calculated to be 63% and 89% at 1.0 and 1.5 mA cm^{-2}, respectively through the comparison between multi-PEO-LiF/ConSPE and multi-PEO-LiT/ConSPE. Both contributions from the sacrificial layer and stabilized SEI were increased when the current density was increased from 1.0 mA cm^{-2} to 1.5 mA cm^{-2}, highlighting

a more significant improvement in the cycling lifetime under a *higher* current density. To further verify the contribution of stabilized SEI effect from LiFSI, the cycling performance of ConSPE with LiFSI (denoted as ConSPE-LiF) was also tested. As shown in **Figure S4**, t_{sc} for ConSPE-LiF is 107 h under the current density of 1.5 mA cm^{-2}, 110% higher than ConSPE with LiTFSI (**Figure 1k**, 51 h), which is slightly lower than the performance improvement from sacrificial layer effect (118%). This is further evidence that the contribution of stabilized SEI effect is close to or lower than that of sacrificial layer effect.

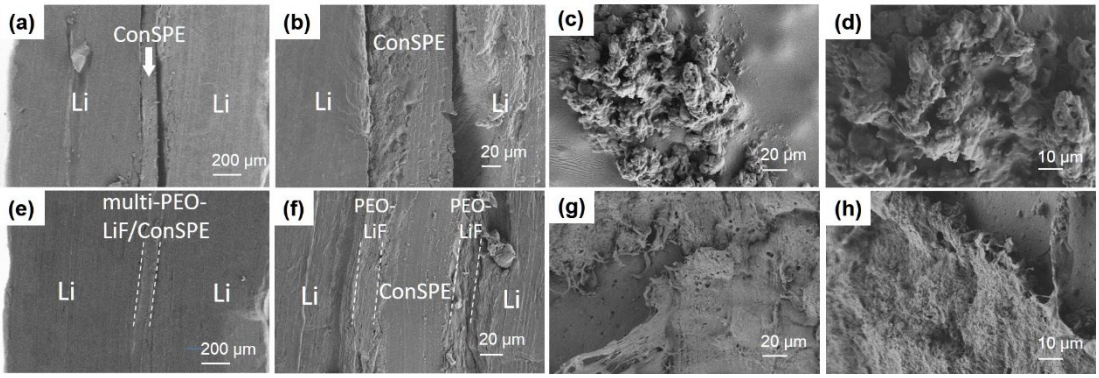

Figure 3. SEM images of symmetrical lithium cells after cycling at 90 °C under 1.5 mA cm^{-2} with an areal capacity of 4.5 mAh cm^{-2}: (a,b) cross-section and (c,d) lithium electrode surface for single-layer ConSPE; (e,f) cross-section and (g,h) lithium electrode surface for multi-PEO-LiF/ConSPE.

The symmetrical lithium cells after cycling were disassembled and investigated with scanning electron microscopy (SEM) and X-ray photoelectron spectroscopy (XPS) to check the lithium and SPE surface morphology and the interface chemistry. Compared with the single-layer ConSPE (**Figure 3a,b**), multi-PEO-LiF/ConSPE showed a more intimate contact and binding with the lithium electrodes (**Figure 3e,f**), which is important for lowering the interfacial resistance and the overpotential (**Figure 4**) during the cell cycling. The lithium electrode surface for the single-layer

ConSPE (**Figure 3c,d**) exhibited nodular lithium deposition after cycled under a high current density of 1.5 mA cm^{-2}. While for multi-PEO-LiF/ConSPE (**Figure 3g,h**), the deposited lithium formed a smoother and more compact layer together with the PEO SPE, which further confirms our sacrificial layer hypothesis. SEM images in **Figure S5** show that the surface of ConSPE in the cell with single-layer ConSPE is rough, with several large lithium aggregations. While the surface of ConSPE in the cell with multilayered SPE is smoother. Combining with SEM images of lithium electrode surface in **Figure 3g,h**, the proposed mechanism for the sacrificial layer in **Figure 2d** could be further verified. Because of the relatively small thickness of the sacrificial layers, for the multilayered SPE, the lithium dendrites are confined in the PEO SPE, forming a smooth and compact layer on the lithium electrode surface (**Figure 3g,h**). XPS spectra in **Figure S6** and atomic abundance in **Table S1** show that the SEI for ConSPE and multi-PEO-LiT/ConSPE exhibit similar components containing C-C, C-OR, COOR, Li_2CO_3, LiOH, Li_2O, and LiF; while for multi-PEO-LiF/ConSPE, the content of LiF and nitrogen/sulfur compounds in the SEI is higher, which is the origin of stabilized SEI from FSI^- anions.

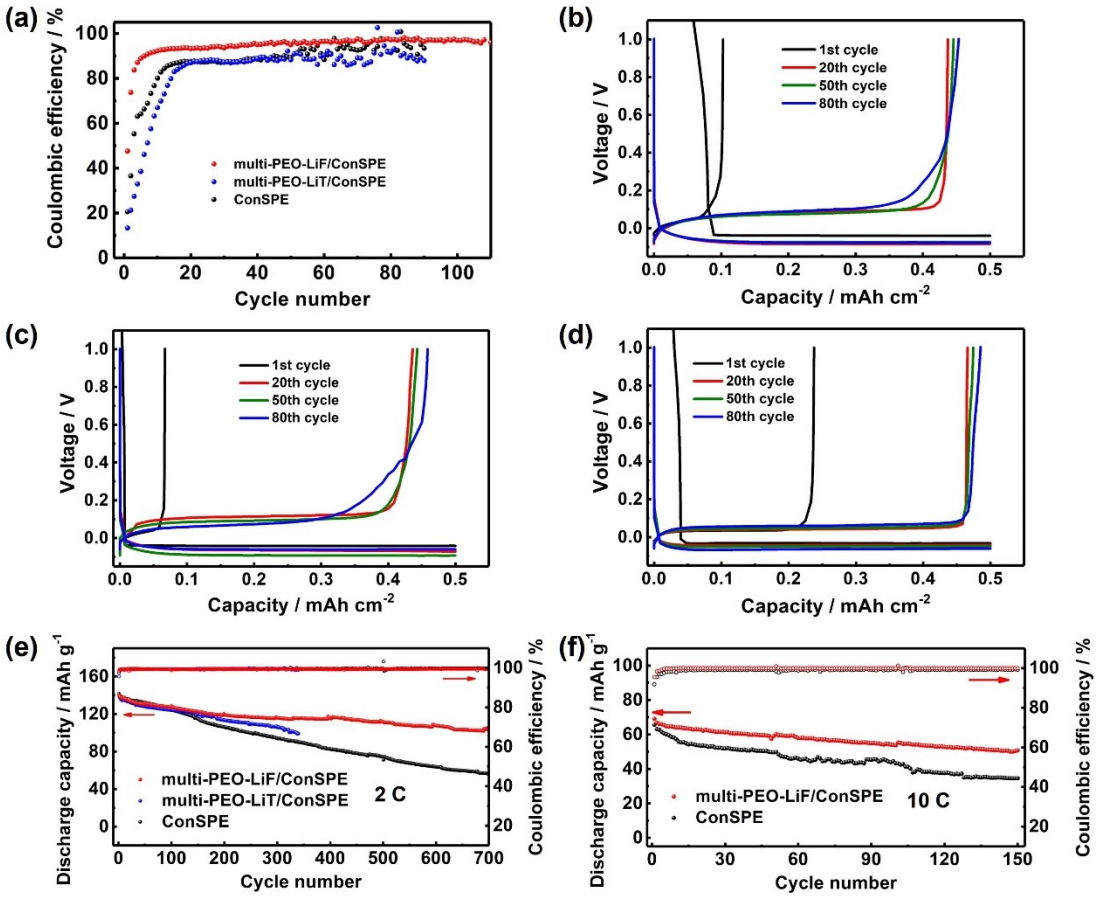

Figure 4. (a-d) Lithium plating-stripping performance on a Cu electrode at 90 °C under 0.5 mA cm^{-2} with an areal capacity of 0.5 mAh cm^{-2}: (a) Coulombic efficiency and voltage profiles for (b) single-layer ConSPE, (c) multi-PEO-LiT/ConSPE and (d) multi-PEO-LiF/ConSPE. (e-f) Li/$LiFePO_4$ battery performance of single-layer ConSPE and multi-PEO-LiF/ConSPE at 90 °C under (a) 2 C and (b) 10 C rate.

Li|Cu cells with these SPEs were assembled to further investigate their lithium plating-stripping behavior. A current density of 0.5 mA cm^{-2} with an areal capacity of 0.5 mAh cm^{-2} was employed in the test. As shown in **Figure 4a**, the Coulombic efficiency (CE) of the lithium plating-stripping for the single-layer ConSPE and multi-PEO-LiT/ConSPE reached about 88% after the initial

interface optimization of about 15 cycles and then started to fluctuate after 50 cycles, indicating that the SEI formed on the Cu surface became unstable and there was continuous SEI decomposition/formation or dead lithium.[2, 34] For multi-PEO-LiF/ConSPE, due to the well-formed SEI, the CE could stabilize at around 97% even after 100 cycles, showing excellent performance among the previously reported SPEs (**Table S2**). The overpotential of the plating-stripping profiles for multi-PEO-LiF/ConSPE (48 mV at 50th cycle, **Figure 4d**) is also lower than those of the single-layer ConSPE (75 mV at 50th cycle, **Figure 4b**) and multi-PEO-LiT/ConSPE (93 mV at 50th cycle, **Figure 4c**), further confirming the favorable SEI with low resistance between the electrode and electrolyte.[39-41] Moreover, the deposited lithium on the Cu electrode surfaces after plating for the single-layer ConSPE (**Figure S7a,b**) and multi-PEO-LiT/ConSPE (**Figure S7c,d**) showed a rough and granular morphology; while the Cu electrode surface for multi-PEO-LiF/ConSPE (**Figure S7e,f**) was more flat and composed of monoliths, demonstrating that the PEO-LiF SPE can homogenize the lithium electrodeposition. The comparison among three SPEs also suggests that the excellent CE of multi-PEO-LiF/ConSPE arises from the favorable SEI from LiFSI rather than the sacrificial layer effect.

To evaluate the effect of the introduced PEO-LiF SPE on the practical LMB performance, Li/$LiFePO_4$ batteries were assembled and tested with the single-layer ConSPE and multi-PEO-LiF/ConSPE. Compared with the single-layer SPE, multi-PEO-LiF/ConSPE shows a slightly higher ionic conductivity (0.99 vs. 0.85 mS cm^{-1}) at 90 °C (**Figure S8**), and higher lithium ion transference number (0.29 vs. 0.19); while the anodic stability is reduced (**Figure S9**) due to introduced PEO-LiF layers. Even so, the oxidation voltage of 4.5 V versus Li/Li^+ for the multilayered SPE can ensure the successful application of $LiFePO_4$ cathode. As shown in **Figure 4e**, when cycled at 90 °C under a 2 C rate, the battery with the single-layer ConSPE delivered an

initial discharge capacity of 141.7 mAh g^{-1} with a capacity retention of 39.8% after 700 cycles; for multi-PEO-LiF/ConSPE, the initial discharge capacity was 140.0 mAh g^{-1}, and the capacity retention after 700 cycles could be 74.6%, which is nearly twice as high as that for single-layer ConSPE. The cycle life, defined as when the capacity retention is reduced to 80%,[42] is 473 cycles for multi-PEO-LiF/ConSPE, which is threefold that for single-layer ConSPE (155 cycles), and also higher than that for multi-PEO-LiT/ConSPE (220 cycles). When tested at an even higher rate of 10 C (**Figure 4f**), the battery with multi-PEO-LiF/ConSPE could still deliver stable cycling, with an initial discharge capacity of 69.1 mAh g^{-1}, and capacity retention of 73.5% after 150 cycles, which is also significantly higher than that for the single-layer ConSPE (52.6%). The battery performance of the multilayered SPE is also superior to that of previously reported SPEs, representing the state-of-the-art (**Table S3**). To the best of our knowledge, this is the first report on solvent-free SPE that delivers stable cycling at such a high current rate. This excellent battery performance for the multilayered SPE can be attributed to its superior lithium dendrite resistance and stabilized SEI formed on the lithium anode, both arise from the sacrificial polymer layer design.

4. Conclusions

In this work, we developed a new design platform of multilayered SPE with polymer sacrificial coating, which directs the growth of lithium dendrites within the sacrificial layer and delays cell short-circuit. Symmetrical lithium cells with the multilayered SPE exhibited more stable cycling with a significantly extended t_{sc} of 801 and 210 h at 1.0 and 1.5 mA cm^{-2}, respectively, which is 2.6 and 4.1 times that for the single-layer ConSPE. The performance improvement is attributed to the synergistic effect of the sacrificial layer and stabilized SEI, which was confirmed by SEM and

lithium plating-stripping tests. Li/SPE/$LiFePO_4$ LMBs with the multilayered SPE delivered significantly more stable cycling at high C-rates of 2 C and 10 C, demonstrating that this novel multilayered SPE concept opens a gateway to new SPE design for LMB applications.

ASSOCIATED CONTENT

Supporting Information

The following file is available free of charge.

DSC curves; voltage-time profiles of symmetrical Li cells; SEM images of cycled ConSPE surface; XPS spectra for Li electrode surface; SEM images of Cu electrode surfaces; comparison of Li-Cu cell performance and Li/$LiFePO_4$ battery performance with previously reported solid polymer electrolytes (Word)

AUTHOR INFORMATION

Corresponding Author

*E-mail: chrisli@drexel.edu, orcid.org/0000-0003-2431-7099

Author Contributions

The manuscript was written through contributions of all authors. All authors have given approval to the final version of the manuscript.

Notes

The authors declare no competing financial interest.

ACKNOWLEDGMENT

We are grateful for the support from the National Science Foundation through Grants CBET 1603520 and CBET 2033882, and the Senior Talents Fund of Jiangsu University (5501220011).

REFERENCES

(1) Liu, J.; Bao, Z.; Cui, Y.; Dufek, E. J.; Goodenough, J. B.; Khalifah, P.; Li, Q.; Liaw, B. Y.; Liu, P.; Manthiram, A.; Meng, Y. S.; Subramanian, V. R.; Toney, M. F.; Viswanathan, V. V.; Whittingham, M. S.; Xiao, J.; Xu, W.; Yang, J.; Yang, X.-Q.; Zhang, J.-G. Pathways for Practical High-Energy Long-Cycling Lithium Metal Batteries. *Nat. Energy* **2019,** *4*, 180-186.

(2) Lin, D.; Liu, Y.; Cui, Y. Reviving the Lithium Metal Anode for High-Energy Batteries. *Nat. Nanotechnol.* **2017,** *12*, 194-206.

(3) Markevich, E.; Salitra, G.; Chesneau, F.; Schmidt, M.; Aurbach, D. Very Stable Lithium Metal Stripping–Plating at a High Rate and High Areal Capacity in Fluoroethylene Carbonate-Based Organic Electrolyte Solution. *ACS Energy Lett.* **2017,** *2*, 1321-1326.

(4) Qian, J.; Henderson, W. A.; Xu, W.; Bhattacharya, P.; Engelhard, M.; Borodin, O.; Zhang, J.-G. High Rate and Stable Cycling of Lithium Metal Anode. *Nat. Commun.* **2015,** *6*, 6362.

(5) Lu, Y.; Tu, Z.; Archer, L. A. Stable Lithium Electrodeposition in Liquid and Nanoporous Solid Electrolytes. *Nat. Mater.* **2014,** *13*, 961-969.

(6) Basile, A.; Bhatt, A. I.; O'Mullane, A. P. Stabilizing Lithium Metal Using Ionic Liquids for Long-Lived Batteries. *Nat. Commun.* **2016,** *7*, 11794.

(7) Ryou, M.-H.; Lee, Y. M.; Lee, Y.; Winter, M.; Bieker, P. Mechanical Surface Modification of Lithium Metal: Towards Improved Li Metal Anode Performance by Directed Li Plating. *Adv. Funct. Mater.* **2015,** *25*, 834-841.

(8) Luo, J.; Lee, R.-C.; Jin, J.-T.; Weng, Y.-T.; Fang, C.-C.; Wu, N.-L. A Dual-Functional Polymer Coating on a Lithium Anode for Suppressing Dendrite Growth and Polysulfide Shuttling in Li–S Batteries. *Chem. Commun.* **2017,** *53*, 963-966.

(9) Lopez, J.; Pei, A.; Oh, J. Y.; Wang, G.-J. N.; Cui, Y.; Bao, Z. Effects of Polymer Coatings on Electrodeposited Lithium Metal. *J. Am. Chem. Soc.* **2018,** *140*, 11735-11744.

(10) Zheng, G.; Lee, S. W.; Liang, Z.; Lee, H.-W.; Yan, K.; Yao, H.; Wang, H.; Li, W.; Chu, S.; Cui, Y. Interconnected Hollow Carbon Nanospheres for Stable Lithium Metal Anodes. *Nat. Nanotechnol.* **2014,** *9*, 618-623.

(11) Khurana, R.; Schaefer, J. L.; Archer, L. A.; Coates, G. W. Suppression of Lithium Dendrite Growth Using Cross-Linked Polyethylene/Poly(Ethylene Oxide) Electrolytes: A New Approach for Practical Lithium-Metal Polymer Batteries. *J. Am. Chem. Soc.* **2014,** *136*, 7395-7402.

(12) Zhou, W.; Wang, S.; Li, Y.; Xin, S.; Manthiram, A.; Goodenough, J. B. Plating a Dendrite-Free Lithium Anode with a Polymer/Ceramic/Polymer Sandwich Electrolyte. *J. Am. Chem. Soc.* **2016,** *138*, 9385-9388.

(13) Pan, Q.; Smith, D. M.; Qi, H.; Wang, S.; Li, C. Y. Hybrid Electrolytes with Controlled Network Structures for Lithium Metal Batteries. *Adv. Mater.* **2015,** *27*, 5995-6001.

(14) Zheng, Y.; Li, X.; Li, C. Y. A Novel De-Coupling Solid Polymer Electrolyte Via Semi-Interpenetrating Network for Lithium Metal Battery. *Energy Storage Mater.* **2020,** *29*, 42-51.

(15) Li, X.; Zheng, Y.; Pan, Q.; Li, C. Y. Polymerized Ionic Liquid-Containing Interpenetrating Network Solid Polymer Electrolytes for All-Solid-State Lithium Metal Batteries. *ACS Appl. Mater. Interfaces* **2019,** *11*, 34904-34912.

(16) Li, X.; Zheng, Y.; Li, C. Y. Dendrite-Free, Wide Temperature Range Lithium Metal Batteries Enabled by Hybrid Network Ionic Liquids. *Energy Storage Mater.* **2020,** *29*, 273-280.

(17) Li, X.; Cheng, S.; Zheng, Y.; Li, C. Y. Morphology Control in Semicrystalline Solid Polymer Electrolytes for Lithium Batteries. *Mol. Syst. Des. Eng.* **2019,** *4*, 793-803.

(18) Zheng, Y.; Li, X.; Fullerton, W. R.; Qian, Q.; Shang, M.; Niu, J.; Li, C. Y. Interpenetrating Network-Based Hybrid Solid and Gel Electrolytes for High Voltage Lithium Metal Batteries. *ACS Appl. Energy Mater.* **2021**, DOI: 10.1021/acsaem.1c00451.

(19) Liu, Y.; Lin, D.; Liang, Z.; Zhao, J.; Yan, K.; Cui, Y. Lithium-Coated Polymeric Matrix as a Minimum Volume-Change and Dendrite-Free Lithium Metal Anode. *Nat. Commun.* **2016,** *7*, 10992.

(20) Lu, L.-L.; Ge, J.; Yang, J.-N.; Chen, S.-M.; Yao, H.-B.; Zhou, F.; Yu, S.-H. Free-Standing Copper Nanowire Network Current Collector for Improving Lithium Anode Performance. *Nano Lett.* **2016,** *16*, 4431-4437.

(21) Cheng, X.-B.; Hou, T.-Z.; Zhang, R.; Peng, H.-J.; Zhao, C.-Z.; Huang, J.-Q.; Zhang, Q. Dendrite-Free Lithium Deposition Induced by Uniformly Distributed Lithium Ions for Efficient Lithium Metal Batteries. *Adv. Mater.* **2016,** *28*, 2888-2895.

(22) Zhao, Q.; Stalin, S.; Zhao, C.-Z.; Archer, L. A. Designing Solid-State Electrolytes for Safe, Energy-Dense Batteries. *Nat. Rev. Mater.* **2020,** *5*, 229-252.

(23) Manthiram, A.; Yu, X.; Wang, S. Lithium Battery Chemistries Enabled by Solid-State Electrolytes. *Nat. Rev. Mater.* **2017,** *2*, 16103.

(24) Lopez, J.; Mackanic, D. G.; Cui, Y.; Bao, Z. Designing Polymers for Advanced Battery Chemistries. *Nat. Rev. Mater.* **2019,** *4*, 312-330.

(25) Xu, H.; Zhang, H.; Ma, J.; Xu, G.; Dong, T.; Chen, J.; Cui, G. Overcoming the Challenges of 5 V Spinel $LiNi_{0.5}Mn_{1.5}O_4$ Cathodes with Solid Polymer Electrolytes. *ACS Energy Lett.* **2019,** *4*, 2871-2886.

(26) Jang, I. C.; Ida, S.; Ishihara, T. Surface Coating Layer on Li Metal for Increased Cycle Stability of Li – O_2 Batteries. *J. Electrochem. Soc.* **2014,** *161*, A821-A826.

(27) Zhu, B.; Jin, Y.; Hu, X.; Zheng, Q.; Zhang, S.; Wang, Q.; Zhu, J. Poly(Dimethylsiloxane) Thin Film as a Stable Interfacial Layer for High-Performance Lithium-Metal Battery Anodes. *Adv. Mater.* **2017,** *29*, 1603755.

(28) Zheng, G.; Wang, C.; Pei, A.; Lopez, J.; Shi, F.; Chen, Z.; Sendek, A. D.; Lee, H.-W.; Lu, Z.; Schneider, H.; Safont-Sempere, M. M.; Chu, S.; Bao, Z.; Cui, Y. High-Performance Lithium Metal Negative Electrode with a Soft and Flowable Polymer Coating. *ACS Energy Lett.* **2016,** *1*, 1247-1255.

(29) Liu, K.; Pei, A.; Lee, H. R.; Kong, B.; Liu, N.; Lin, D.; Liu, Y.; Liu, C.; Hsu, P.-c.; Bao, Z.; Cui, Y. Lithium Metal Anodes with an Adaptive "Solid-Liquid" Interfacial Protective Layer. *J. Am. Chem. Soc.* **2017,** *139*, 4815-4820.

(30) Cheng, X.-B.; Zhang, Q. Dendrite-Free Lithium Metal Anodes: Stable Solid Electrolyte Interphases for High-Efficiency Batteries. *J. Mater. Chem. A* **2015,** *3*, 7207-7209.

(31) Li, X.; Zheng, Y.; Duan, Y.; Shang, M.; Niu, J.; Li, C. Y. Designing Comb-Chain Crosslinker-Based Solid Polymer Electrolytes for Additive-Free All-Solid-State Lithium Metal Batteries. *Nano Lett.* **2020,** *20*, 6914-6921.

(32) Monroe, C.; Newman, J. The Impact of Elastic Deformation on Deposition Kinetics at Lithium/Polymer Interfaces. *J. Electrochem. Soc.* **2005,** *152*, A396-A404.

(33) Hallinan, D. T.; Mullin, S. A.; Stone, G. M.; Balsara, N. P. Lithium Metal Stability in Batteries with Block Copolymer Electrolytes. *J. Electrochem. Soc.* **2013,** *160*, A464-A470.

(34) Cheng, X.-B.; Zhang, R.; Zhao, C.-Z.; Zhang, Q. Toward Safe Lithium Metal Anode in Rechargeable Batteries: A Review. *Chem. Rev.* **2017,** *117*, 10403-10473.

(35) Zhang, X.; Wang, S.; Xue, C.; Xin, C.; Lin, Y.; Shen, Y.; Li, L.; Nan, C.-W. Self-Suppression of Lithium Dendrite in All-Solid-State Lithium Metal Batteries with Poly(Vinylidene Difluoride)-Based Solid Electrolytes. *Adv. Mater.* **2019,** *31*, 1806082.

(36) Aldalur, I.; Martinez-Ibañez, M.; Piszcz, M.; Rodriguez-Martinez, L. M.; Zhang, H.; Armand, M. Lowering the Operational Temperature of All-Solid-State Lithium Polymer Cell with Highly Conductive and Interfacially Robust Solid Polymer Electrolytes. *J. Power Sources* **2018,** *383*, 144-149.

(37) Camacho-Forero, L. E.; Smith, T. W.; Balbuena, P. B. Effects of High and Low Salt Concentration in Electrolytes at Lithium–Metal Anode Surfaces. *J. Phys. Chem. C* **2017,** *121*, 182-194.

(38) Zhang, H.; Liu, C.; Zheng, L.; Xu, F.; Feng, W.; Li, H.; Huang, X.; Armand, M.; Nie, J.; Zhou, Z. Lithium Bis(Fluorosulfonyl)Imide/Poly(Ethylene Oxide) Polymer Electrolyte. *Electrochim. Acta* **2014,** *133*, 529-538.

(39) Xiao, L.; Zeng, Z.; Liu, X.; Fang, Y.; Jiang, X.; Shao, Y.; Zhuang, L.; Ai, X.; Yang, H.; Cao, Y.; Liu, J. Stable Li Metal Anode with "Ion–Solvent-Coordinated" Nonflammable Electrolyte for Safe Li Metal Batteries. *ACS Energy Lett.* **2019,** *4*, 483-488.

(40) Zeng, Z.; Murugesan, V.; Han, K. S.; Jiang, X.; Cao, Y.; Xiao, L.; Ai, X.; Yang, H.; Zhang, J.-G.; Sushko, M. L.; Liu, J. Non-Flammable Electrolytes with High Salt-to-Solvent Ratios for Li-Ion and Li-Metal Batteries. *Nat. Energy* **2018,** *3*, 674-681.

(41) Qiu, F.; Li, X.; Deng, H.; Wang, D.; Mu, X.; He, P.; Zhou, H. A Concentrated Ternary-Salts Electrolyte for High Reversible Li Metal Battery with Slight Excess Li. *Adv. Energy Mater.* **2019,** *9*, 1803372.

(42) Pan, Q.; Barbash, D.; Smith, D. M.; Qi, H.; Gleeson, S. E.; Li, C. Y. Correlating Electrode–Electrolyte Interface and Battery Performance in Hybrid Solid Polymer Electrolyte-Based Lithium Metal Batteries. *Adv. Energy Mater.* **2017,** *7*, 1701231.

Table of Contents graphic